ACS Sustainable Chemistry & Engineering

Research Article

pubs.acs.org/journal/ascecg

Electrochemical Conversion of Muconic Acid to Biobased Diacid Monomers

John E. Matthiesen,[†,‡,∥] Jack M. Carraher,[†,‡,∥] Monica Vasiliu,[§] David A. Dixon,[§] and Jean-Philippe Tessonnier*[,†,‡,∥]

[†]Department of Chemical and Biological Engineering, Iowa State University, 618 Bissell Road, Ames, Iowa 50011, United States
[‡]NSF Engineering Research Center for Biorenewable Chemicals (CBiRC), 617 Bissell Road, Ames, Iowa 50011, United States
[∥]U.S. Department of Energy Ames Laboratory, 2408 Pammel Drive, Ames, Iowa 50011, United States
[§]Department of Chemistry, The University of Alabama, Shelby Hall, Tuscaloosa, Alabama 35487, United States

Supporting Information

ABSTRACT: Electrocatalysis is evolving as a competitive alternative to conventional heterogeneous catalysis for the conversion of platform chemicals from biomass. Here, we demonstrate the electrocatalytic conversion of *cis,cis*-muconic acid, a fermentation product, to *trans,trans*-muconic acid, *trans*-3-hexenedioic acid, and adipic acid used for the production of biobased polyamides and polyesters such as nylon, nylon derivatives, and polyethylene terephthalate (PET). The electrocatalytic hydrogenation in this work considers a wide range of early, late, and post-transition metals (Cu, Fe, Ni, Mo, Pb, Pd, Sn, and Zn) with low and high hydrogen overpotentials, and varying degrees of metal hydrogen binding strengths. The binding strength was determined to be an important factor for the conversion rate, faradaic efficiency, and product distribution. Selectivities are also discussed in relation to thermodynamic data, which suggests the possibility to tune the kinetics of the reaction to allow for the variable production of multiple biobased monomers.

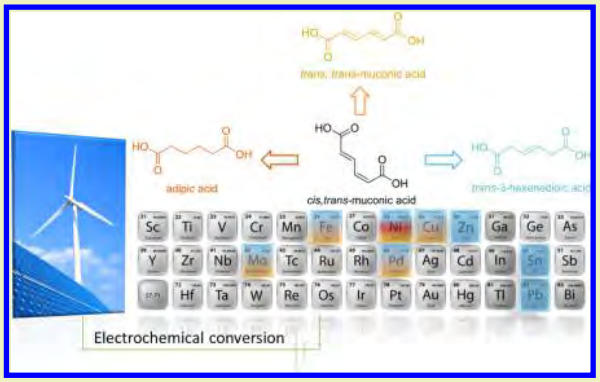

KEYWORDS: *Electrocatalysis, Electrochemistry, Muconic acid, Hydrogenation, Renewables, Polyamides, Adipic acid, Hexenedioic acid*

INTRODUCTION

The production of renewable chemicals from biomass has significantly evolved in recent years and numerous processes have either reached a commercial stage or are close to commercialization.[1] In 2010, the U.S. Department of Energy published an updated "Top 10" list of biomass derived platform chemicals. This list and its predecessor have played a critical role in both the identification of the most promising compounds and as a guiding factor for the research in the field.[2,3] As anticipated in these publications, biocatalysis and chemical catalysis have been equally important. Carbohydrates have been converted to 5-hydroxymethylfurfural (HMF), 2,5-furandicarboxylic acid (FDCA), levulinic acid, 2,5-dimethylfuran (DMF), furfural, and their derivatives using heterogeneous catalysts.[4−6] At the same time, microorganisms were metabolically engineered to selectively produce platform acids by fermentation. Notably, lactic, itaconic, succinic, fumaric, and malic acids were obtained with high yield and titer.[1,7] So far, advances in bio- and chemical catalysis occurred simultaneously and independently from each other. However, coupling the two approaches grants access to new conversion pathways or new molecules that are not available from petroleum, thus providing the chemical industry with new building blocks.[8−17]

Muconic acid (MA) is not included in the DOE "Top 10" list, but is receiving increasing attention for the sustainable production of adipic acid (AA) and other important monomers from biomass.[18−21] This new interest in MA is due to the increasing market size of AA, which is expected to grow 3−5% per year until 2020,[22,23] and the need for greener processes for AA synthesis. AA is still produced by the sequential oxidation of cyclohexane using air and nitric acid as reactants, releasing N_2O to the atmosphere.[19] Several large companies developed processes to recycle N_2O or catalytically convert it to harmless N_2 and O_2.[24] However, simple mitigation of environmental effects does not address all of the issues associated with this production method. Therefore, efforts are also being dedicated to develop alternative AA production routes that are more sustainable.[19]

MA is synthesized from glucose or lignin by fermentation using metabolically engineered bacteria (*Pseudomonas putida*, *Escherichia coli*) or yeast (*Saccharomyces cerevisiae*).[12,20] Over the past 5 years, MA emerged as a promising platform molecule

Received: April 3, 2016
Revised: May 1, 2016
Published: May 3, 2016

DOI: 10.1021/acssuschemeng.6b00679
ACS Sustainable Chem. Eng. 2016, 4, 3575−3585

Scheme 1. Value-Added Products Obtained from Biobased Muconic Acid

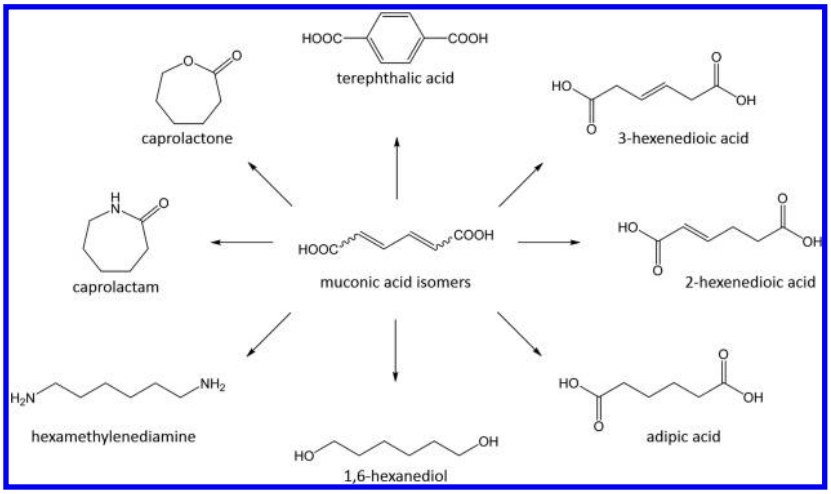

due to increased titers and potential for further diversification through heterogeneous catalysts.[20,25] The highest titer to date was achieved with an engineered *E. coli* strain able to produce 59.2 g L^{-1} at a 30% mol/mol glucose yield under fed-batch culture.[22] In addition, Vardon et al. produced 13.5 g L^{-1} muconate using engineered *P. putida* and a lignin-derived model compound as a feedstock.[12]

Once purified, biologically produced *cis,cis*-MA (*cc*MA) can be converted to large scale commodity chemicals such as adipic acid, 1,6-hexanediol, hexamethylenediamine, caprolactone, and caprolactam, which are important building blocks for the manufacture of Nylon-6, Nylon-6,6, and other polyesters and polyurethanes (Scheme 1).[18] It was also demonstrated that *cc*MA can be isomerized to *trans,trans*-MA (*tt*MA) and further reacted to terephthalic acid, a key building block for the production of polyethylene terephthalate (PET).[23] Many of these conversions involve a hydrogenation step under high pressure (2−24 bar) in the presence of an expensive precious metal catalyst. For example, *cc*MA was hydrogenated to AA under 24 bar H_2 over a Pd/C catalyst.[12] To be truly sustainable, it would be beneficial to substitute precious metals for Earth-abundant catalysts such as Ni, Cu, Zn, or Pb, organic solvents for water, and external hydrogen for hydrogen generated *in situ* in accordance with a green methodology.[26]

Electrocatalytic hydrogenations (ECH) have recently emerged as a promising approach to hydrogenate renewable chemicals in water under ambient conditions.[27−34] For example, we have demonstrated the ECH of MA directly in the fermentation broth, eliminating an entire separation step that typically occurs prior to the chemical hydrogenation.[15] ECH usually proceeds by applying a −0.3 to −1.8 V potential on a transition metal electrode. In contrast to high-pressure hydrogenation, hydrogen is generated *in situ* from water, at the surface of the catalyst, thus eliminating H_2 mass transfer limitations and the need for high pressure.[35] Cheap Earth-abundant metals such as Ni, Cu, and Pb were shown to be particularly active and selective for the ECH of biobased levulinic acid to valeric acid and HMF to DMF.[27,28,30−32] Furthermore, the selectivity of the catalyst was tuned by varying the pH and the applied potential. For example, 95% selectivity to valeric acid was achieved for Pb at −1.5 V and pH 0, but 100% selectivity to γ-valerolactone (GVL) was obtained for the same catalyst at −1.3 V and pH 7.5.[31] Although ECH is not a mature technology, its large tunability offers unique advantages when considering industrial applications. This is particularly relevant for reactions that display high yields while requiring low energy inputs and space times over their heterogeneous catalytic counterpart.

Herein, we report on the electrocatalytic conversion of MA under ambient temperature and pressure over a wide range of early, late, and post-transition metal catalysts. Reaction conditions and pure metal catalyst composition were varied in an attempt to identify the key parameters that govern ECH selectivity and favor ECH over hydrogen evolution (HER). We analyze the obtained results in the light of previous studies performed on HER and discuss the importance of the free energy for hydrogen adsorption ΔG_H on ECH performance. Finally, we show that the reaction conditions can be tuned to control the product distribution and generate compounds that are not observed during high-pressure hydrogenation. Specifically, high selectivities to *trans*-3-hexenedioic acid (*t*3HDA), a biobased chemical rarely observed and only in low yields during the semihydrogenation of MA under pressurized H_2, and *trans,trans*-MA (*tt*MA) were achieved using base metal electrocatalysts.[36]

EXPERIMENTAL SECTION

Electrocatalysis. The electrochemical studies were conducted in a conventional single compartment three-electrode glass cell using a BioLogic potentiostat (VSP-300). All potentials are in reference to the reversible hydrogen electrode (RHE). Initial experiments used to propose reaction schemes and investigate product decomposition were performed with 11 mL solution of *cis,trans*-muconic acid (*ct*MA) dissolved in 0.01 M sulfuric acid (H_2SO_4) as an electrolyte. The cell was equipped with a Pt counter electrode (Biologic), a Ag/AgCl in NaCl reference electrode (Biologic), and a 10 cm^2 Pb rod (Rotometals, 99.9% purity) working electrode. The solutions were magnetically stirred at 700 rpm with a PTFE flea stir bar. During chronoamperometry experiments, 0.5 mL aliquots of the reaction medium were withdrawn periodically.

Catalyst screenings were conducted with 50 mL solutions of 3.52 mM *ct*MA and 0.26 M formic acid (electrolyte). Formic acid was preferred over sulfuric acid to more closely resemble the hydrogenation of MA in a fermentation broth and for ease in preparation for product analysis by ultra performance liquid chromatography coupled mass spectrometry (UPLC-MS). The cell was equipped with an Ag/AgCl in sat. KCl reference electrode (Pine) and Pt counter electrode (Pine Research Instruments). The working electrodes were purchased as follows: Sigma (Pd, Mo), Flinn Scientific (Cu, Fe, Pb, Zn), and Science Company (Ni). Geometric surface areas are displayed in Table

DOI: 10.1021/acssuschemeng.6b00679
ACS Sustainable Chem. Eng. 2016, 4, 3575−3585

S1. Prior to electrocatalysis, the electrodes were cleaned with acetone and Milli-Q water, and wiped with a Kimwipe. All solutions were magnetically stirred at 400 rpm with a PTFE octagonal stir bar for the duration of the catalytic test. During chronoamperometry experiments, 0.5 mL aliquots of the reaction medium were collected at 5, 15, 30, and 60 min for analysis.

Electropolishing was conducted in a two-electrode electrochemical cell following ASTM E3 standards using a TiO_2 electrode strip as the counter electrode.[37] A potential of 15 V was applied for 20 s. The Pb electrode was subsequently reduced in a 0.5 M sulfuric acid solution.

Product Analysis. Samples were diluted 1:1 with Milli-Q water (18.2 MΩ) and then analyzed with a Waters Acquity H-Class ultra performance liquid chromatography (UPLC) instrument equipped with photodiode array (PDA) and QDa mass detectors. A Waters HSS C18 1.8 μm (2.1 × 100 mm) column was used to separate *ct*MA, *tt*MA, *t*3HDA, and AA. The MA isomers were quantified with the PDA detector set at 230 nm whereas *t*3HDA and AA were quantified with the QDa mass detector in positive and negative mode, respectively. ACS grade *cc*MA, *tt*MA, *t*3HDA, and AA were purchased from Sigma (St Louis, MO). These compounds were used for UPLC calibration and as references for NMR analysis. *ct*MA was prepared by heating *cc*MA at 75 °C for 25 min. Reactant and product elution times corresponding to the analysis are found in the Supporting Information (Figure S1).

^{1}H NMR analysis was performed on a Bruker 600 MHz NMR spectrometer (AVIII600). The samples were dried at room temperature under a current of air, reconstituted in deuterium oxide, and subsequently analyzed. Genuine spectra of the reactants and products are found in the Supporting Information (Figure S2).

Optical microscopy images were acquired with an $EVOS_{fl}$ light microscope.

Computational Methods. The geometries were initially optimized using density functional theory (DFT)[38] with the hybrid B3LYP exchange-correlation functional,[39,40] and the DZVP2 basis set.[41] Vibrational frequencies were calculated to ensure that the optimized structures were minima. The optimized B3LYP/DZVP2 geometries were then used as starting points for G3MP2 calculations[42] to predict gas phase enthalpy of formation (ΔH_{gas}) and the gas phase acidity (ΔG_{gas} for the reaction AH → A^- + H^+). These calculations were done with the Gaussian 09 program system.[43]

The enthalpies of formation of the pure liquid phases were estimated using the fact that the free energy is zero at a phase change so that the enthalpy of vaporization (ΔH_{vap}) can be calculated using $\Delta H_{vap} = T_{BP}\,\Delta S_{vap}$, where ΔH_{vap} is the enthalpy of vaporization, T_{BP} is the boiling point in degrees Kelvin (K), and ΔS_{vap} is the entropy of vaporization. ΔS_{vap} is approximately constant for many compounds, as initially found by Pictet and Trouton,[44−48] and thus, for a given boiling point, ΔH_{vap} can be estimated. From our previous calculations for organic acids,[49,50] we found that ΔS_{vap} = 0.031 cal/(mol K). The enthalpy of formation of the pure liquid phase (ΔH_{liq}) is obtained as the difference between the gas enthalpy of formation and the enthalpy of vaporization:

$$\Delta H_{liq} = \Delta H_{gas} - \Delta H_{vap}$$

The COSMO-RS[51−54] approach as implemented in the ADF[55,56] program was used to estimate T_{BP} from DFT results at the B88P86/TZ2P level.[57−59] The solvation component for the acidity calculations were done as follows. The solvation free energies in water at 298 K were calculated using the self-consistent reaction field approach[60] with the COSMO parameters,[52,61] as implemented in the Gaussian 03[62] using the B3LYP/DZVP2 gas phase geometries. For the COSMO (B3LYP/DZVP2) calculations in Gaussian 03, the radii developed by Klamt and co-workers were used to define the cavity.[61] The Gibbs free energy in aqueous solution (ΔG_{aq}) was calculated from $\Delta G_{aq} = \Delta G_{gas} + \Delta\Delta G_{solv}$ where ΔG_{gas} is the gas phase free energy and $\Delta\Delta G_{solv}$ is the aqueous solvation free energy calculated as differences between conjugate base and the acid. A dielectric constant of 78.39 corresponding to that of bulk water was used in the COSMO calculations. The solvation energy is reported as the electrostatic energy (polarized solute − solvent). To improve the calculated values for pK_a, an approach which predicts the pK_a relative to known standards (CH_3COOH) was used.[63] The error in the absolute calculated pK_a of CH_3COOH is 3.0 pK_a units using a value for the free energy of solvation of the proton of −264.3 kcal/mol.[64,65] The pK_a values in aqueous solution relative to CH_3COOH (HA + CH_3COO^- → A^- + CH_3COOH) were calculated using the following:

$$pK_a' = pK_a(CH_3COOH) + \Delta G_{aq}/(2.303RT)$$

The calculations were performed on a Xeon-based Dell Linux cluster at the University of Alabama, and a local AMD Opteron-based and Intel Xeon-based Linux cluster from Penguin Computing.

RESULTS AND DISCUSSION

Muconic Acid Synthesis and Isomerization. Biocatalysts selectively produce *cc*MA by fermentation.[25] However, the *ct* and *tt* isomers of MA are known and the spontaneous formation of *ct*MA from *cc*MA under acidic conditions has been reported previously.[20,66] Therefore, we first investigated the isomerization of *cc*MA at low pH and under ambient conditions to simulate the ECH conditions. A 5 mM solution of *cc*MA with 1.5 mM acetic acid in D_2O was reacted at room temperature (22.5 °C) for 8 days (Figure 1). Periodic analysis

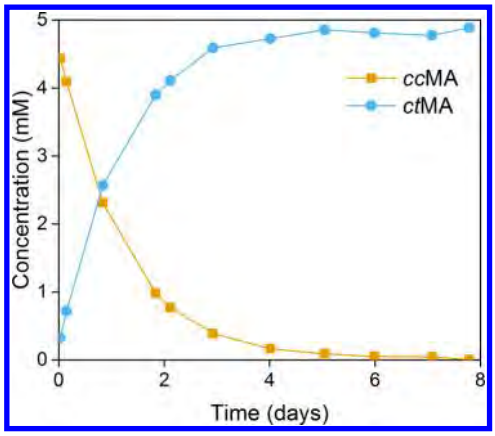

Figure 1. Concentrations of MA isomers over time. Full conversion of *cc*MA to *ct*MA occurs within 3 days at 22.5 °C.

by ^{1}H NMR revealed that *cc*MA isomerization to *ct*MA was nearly complete within 3 days. The composition of the solution remained stable afterward for an additional 5 days, at which time monitoring was ceased. Increasing the temperature to 75 °C allowed the reaction to complete within only 20 min. *tt*MA was never observed in good agreement with previous works, which stated that *tt*MA formation requires chemical activation.[22] Given that *cc*MA production by low pH fermentation with engineered *S. cerevisiae* typically occurs at temperatures >22.5 °C for 3−5 days and the ECH is conducted under acidic conditions, we decided to carry out the present study using the *ct*MA isomer as a reactant.

Mechanistic and Thermodynamic Considerations. During MA hydrogenation, ECH and HER are competitive reactions. Both processes could even share the first elementary step (Volmer step) where protons from the solution are reduced to form adsorbed hydrogen atoms (eq 1).[35] The adsorbed atoms can then either participate in the ECH reaction or combine to generate H_2 following the Tafel or Heyrovsky steps (eqs 2 and 3). Although H_2 is a valuable byproduct, its formation is typically undesired during ECH as it lowers the faradaic efficiency (ratio of electrons consumed by ECH vs HER) and the overall performance of the ECH catalyst.[34,35] In

DOI: 10.1021/acssuschemeng.6b00679
ACS Sustainable Chem. Eng. 2016, 4, 3575−3585

Table 1. Heats of Formation (Gas and Liquid), Boiling Point, and Gas Phase Acidities (ΔG_{gas}) at G3MP2 Level in kcal mol^{-1} and pK_a (Relative to Acetic Acid)

molecule[a]	ΔH_f (0 K) (gas)	ΔH_f (298 K) (gas)	BP calc	$\Delta H_{vap,BP}$	ΔH_f (298 K) (liq)	ΔG_{gas} acidity	first pK_a (exp pK_a)[b]
*cc*MA	−145.8	−150.7	503.2	15.6	−166.3	328.0	2.9
*ct*MA	−146.6	−151.5	569.4	17.7	−169.1	328.7	2.9
*tt*MA	−148.8	−153.6	564.1	17.5	−171.0	329.0	3.4 (2.7)[c]
*t*3HDA	−169.5	−175.9	583.7	18.1	−194.0	333.8	4.4 (3.96)
*c*3HDA	−168.0	−175.5	584.6	18.1	−193.6	329.6	4.5
*t*2HDA	−171.4	−177.8	587.5	18.2	−196.1	332.1	5.3
*c*2HDA	−170.2	−176.8	564.9	17.5	−194.3	335.2	5.9
AA	−197.3	−205.4	586.5	18.2	−223.6	335.2	5.0 (4.43)

[a]Notation: *cc*MA, *ct*MA, and *tt*MA correspond to *cis,cis-*, *cis,trans-*, and *trans,trans*-muconic acid; *c*2HDA, *t*2HDA, *c*3HDA, and *t*3HDA designate the *cis* (*c*) and *trans* (*t*) isomers of 2-hexenedioic acid (2HDA) and 3-hexenedioic acid (3HDA); AA corresponds to adipic acid. [b]Experimental pK_a values found in the literature are provided in brackets for comparison. [c]Value from ref 70.

addition, H_2 does not participate in the hydrogenation reaction; specifically, with the applied potential there is no production of atomic hydrogen from H_2.[67]

$$H^+ + e^- \rightarrow H_{ads} \quad \text{Volmer step (in acid)} \quad (1)$$

$$2H_{ads} \rightarrow H_2 \quad \text{Tafel step} \quad (2)$$

$$H_{ads} + H^+ + e^- \rightarrow H_2 \quad \text{Heyrovsky step (in acid)} \quad (3)$$

Before any further considerations, it is important to study the thermodynamic equilibria associated with HER and ECH to understand how they evolve with pH and applied potential. Thermodynamic data is widely available for HER.[68] However, muconic acid is not a common reactant and, like many biorenewable molecules, thermodynamic data is not available in the open literature.[49,50] Therefore, we calculated the thermodynamic properties of all the molecules susceptible to form as well as the enthalpies of formation and the free energies associated with all the hydrogenation reactions that may take place during ECH (Tables 1 and 2). In all cases, we considered a two-step reaction where MA is first hydrogenated to the corresponding monounsaturated diacid (*cis* and *trans* isomers of 2 and 3HDA) before further hydrogenation to AA (Table 2). As shown in Table 2, all the reactions associated with the hydrogenation of MA to AA are thermodynamically favored by 10 to 20 kcal mol^{-1}. These theoretical values can be further used to calculate the theoretical potential of each reaction and its variation with pH using Nernst's eq (Figure 2). As shown in Figure 2, the potentials for ECH are higher than for HER over the pH range 0−14. As HER and ECH are cathodic reactions, Figure 2 implies that ECH reactions are thermodynamically favored over HER, regardless of pH. The plot also reveals little difference between *t*2HDA, *t*3HDA, and AA, meaning that it may be possible to selectively synthesize any of these 3 chemicals by fine-tuning the reaction kinetics. Although not commonly used for polymer synthesis, we anticipate that 2HDA and 3HDA could become interesting monomers for polyester and polyamide synthesis based on their structural resemblance with adipic and fumaric acids.[69]

Table 2. Hydrogenation Energies at G3MP2 in kcal mol^{-1}

reaction[a]	ΔH_{gas}	ΔG_{gas}	ΔH_{liq}	ΔG_{aq}
*cc*MA + H_2 → *t*3HDA	−24.0	−17.0	−27.6	−20.3
*cc*MA + H_2 → *c*3HDA	−23.6	−13.5	−27.3	−17.1
*cc*MA + H_2 → *t*2HDA	−26.0	−18.4	−29.7	−21.9
*cc*MA + H_2 → *c*2HDA	−24.9	−17.1	−28.0	−19.9
*ct*MA + H_2 → *t*3HDA	−23.3	−15.8	−24.8	−15.9
*ct*MA + H_2 → *c*3HDA	−22.9	−12.3	−24.5	−12.7
*ct*MA + H_2 → *t*2HDA	−25.2	−17.3	−26.9	−17.5
*ct*MA + H_2→ *c*2HDA	−24.2	−15.9	−25.2	−15.5
*tt*MA + H_2 → *t*3HDA	−21.2	−13.8	−22.9	−14.3
*tt*MA + H_2 → *c*3HDA	−20.8	−10.3	−22.5	−11.1
*tt*MA + H_2 → *t*2HDA	−23.1	−15.2	−25.0	−15.9
*tt*MA + H_2 → *c*2HDA	−22.1	−13.9	−23.3	−13.9
*t*3HDA + H_2 → AA	−28.4	−19.3	−29.7	−18.8
*c*3HDA + H_2 → AA	−28.8	−22.7	−30.0	−22.1
*t*2HDA + H_2 → AA	−26.5	−17.8	−27.6	−17.3
*c*2HDA + H_2 → AA	−27.5	−19.1	−29.3	−19.3

[a]Notation: *cc*MA, *ct*MA, and *tt*MA correspond to *cis,cis-*, *cis,trans-*, and *trans,trans*-muconic acid; *c*2HDA, *t*2HDA, *c*3HDA, and *t*3HDA designate the *cis* (*c*) and *trans* (*t*) isomers of 2-hexenedioic acid (2HDA) and 3-hexenedioic acid (3HDA); AA corresponds to adipic acid.

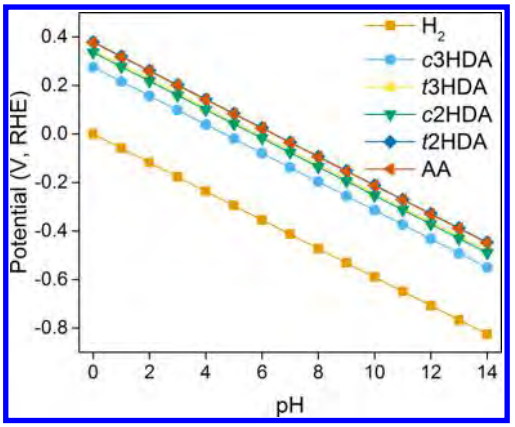

Figure 2. Theoretical potentials for the formation of hydrogen (HER), *c*3HDA, *t*3HDA, *c*2HDA, *t*2HDA, and AA from *ct*MA as a function of pH based on calculated ΔG_{aq} values (Table 2).

Previous work on ECH revealed that poor HER catalysts offer the highest hydrogenation activities.[27−32] Unconventional post-transition metals such as Pb were particularly selective for levulinic acid and HMF hydrogenation. This observation can be rationalized by analyzing the volcano plot published by Greeley et al. for HER.[68] The highest exchange current densities (high HER activity) were observed for metals with a free energy for hydrogen binding $\Delta G_H \sim 0$. Metals that bind hydrogen more strongly ($\Delta G_H < 0$) or more weakly ($\Delta G_H > 0$) are significantly less active for HER and adsorbed hydrogen atoms are therefore more likely to be involved in hydrogenation reactions than H_2

DOI: 10.1021/acssuschemeng.6b00679
ACS Sustainable Chem. Eng. 2016, 4, 3575−3585

evolution (Figure 3, adapted from refs 68 and 71).[35] However, at this point it is unclear whether weak ($\Delta G_H > 0$) or strong

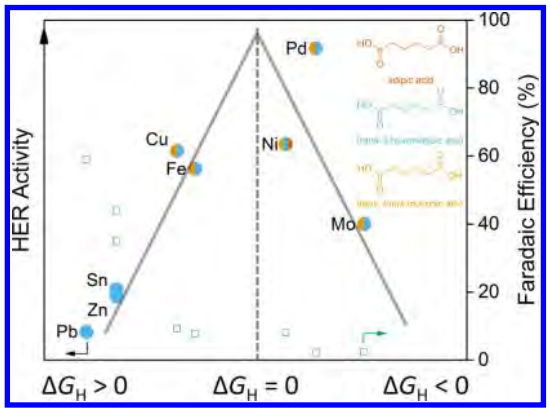

Figure 3. Volcano plot showing the correlation between exchange current densities (HER activities) achieved and the main products formed through ECH as a function of the free energy of hydrogen adsorption ΔG_H of the metals. Optimal HER activity is achieved for metals with $\Delta G_H \sim 0$. For clarity, only the metals tested in the present work are displayed on the plot. The colors indicate the main products formed during ECH (gold, *tt*MA; blue, *t*3HDA; red, AA). The open symbols correspond to the faradaic efficiency for ECH at the end of the reaction duration. Adapted based on refs 68 and 71.

hydrogen binding ($\Delta G_H < 0$) is best suited for ECH and how large $|\Delta G_H|$ must be to ensure optimal hydrogenation activity. The hydrogen binding energy may influence a range of parameters including the hydrogen coverage of the catalyst, the nature and number of metal sites available for MA binding and activation, the activation barrier for ECH, and the availability of hydrogen to react through HER and ECH. These parameters may further influence the HER and ECH rates, the faradaic efficiency, and selectivity to the various *ct*MA hydrogenation products. Therefore, we tested a broad range of early, late, and post-transition metals representative of both the low and high overpotential metals commonly used for ECH.

ECH with Low Hydrogen Overpotential Metals. The results obtained for representative low hydrogen overpotential metals are shown in Figure 4. The catalytic tests were performed at −1.12 and −1.72 V vs RHE. The surface of the bulk metal electrodes remains fully reduced (metallic) under these potentials, as confirmed by the corresponding Pourbaix diagrams.[72−74] In all cases, a solution of 3.52 mM *ct*MA and 0.26 M formic acid was reacted for 1 h and aliquots of the solution were analyzed by UPLC after 5, 15, 30, and 60 min of reaction. As expected, increasing the cathodic potential from −1.12 to −1.72 V increased the kinetics of all the electrocatalytic reduction reactions, hence the kinetics of both ECH and HER. Although ECH reactions are in general thermodynamically favored over HER (e.g., Figure 2),[31] the latter is one of the fastest known electrochemical reactions. As a result, high *ct*MA conversions were measured after 1 h, but the faradaic efficiencies did not exceed 15% for low hydrogen overpotential metals (i.e., good HER catalysts).

These faradaic efficiencies are also consistent with the fact that H^+ and *ct*MA compete to adsorb on the surface of the catalyst and that the concentration of *ct*MA is 2 orders of magnitude lower than $[H^+]$. Faradaic efficiencies of 70−90% were only achieved for the ECH of levulinic acid and HMF when the initial concentrations of the organic reactant and acidic electrolyte were close and the conversion was lower than 10%.[29,31,32] Here, the experiments were carried out with 3.52 mM *ct*MA (500 mg L^{-1}) to represent the highest titer for yeast fermentation[15] and to remain below the solubility limit of the MA isomers (*cc*MA ∼ 1 g L^{-1}, *ct*MA = 5.2 g L^{-1}, *tt*MA = 90 mg L^{-1}). Finally, it should also be mentioned that the solutions were not purged with inert gas before and/or during this set of electrocatalytic reaction. Hence, dissolved oxygen is likely to react at the counter electrode following the oxygen reduction reaction (ORR), which would further lower the FE (*vide infra*). We did not attempt to increase the faradaic efficiency as the primary goal of this work was to elucidate the key parameters that govern conversion and selectivity.

It has been shown previously that the high pressure thermocatalytic hydrogenation of muconic acid with Pt group metals yields adipic acid.[12] However, under our reaction conditions, Ni was the only metal to yield both *t*3HDA and AA. Interestingly, bulk Pd foil did not produce AA even after extended reaction times. In all experiments, the fraction of unknown or undetected products calculated based on the carbon balance remained stable or decreased over time and when increasing the potential from −1.12 to −1.72 V, thus indicating that *ct*MA and/or product decomposition was minimal. As expected for good HER catalysts, the ECH rate was low for Pd and the *ct*MA conversion after 1 h reached 20% at best. Ni, Cu, and Fe were significantly more active than Pd, in good agreement with their position on the volcano plot for HER (Figure 3). *ct*MA conversion ranged between 30 and 60% depending on the metal and applied potential. *t*3HDA was the main product for these catalysts; however, *tt*MA and AA (in the case of Ni) were also detected. The nonfaradaic *ct*MA isomerization to *tt*MA appears to be electrochemically promoted, enhanced by electroreduced protons on the surface of the electrode.[75,76] In addition, the selectivity of *tt*MA remained stable for Cu and slightly decreased over the course of the reaction for Fe, which could indicate that *tt*MA is an intermediate in the hydrogenation of *ct*MA to *t*3HDA (*vide infra*). Overall, although the formation of AA on Ni opens interesting perspectives, the low faradaic efficiencies and low *ct*MA conversion achieved with low overpotential metals represent major drawbacks.

ECH with High Hydrogen Overpotential Metals (Mo, Sn, Zn, Pb). Metals that deviate further from ideal HER catalysts and present large $|\Delta G_H|$ were more selective toward *t*3HDA and showed faster ECH rates than low hydrogen overpotential metals. 40−80% *ct*MA was converted within 1 h on Pb, Sn, and Zn, as shown in Figure 5. The selectivity to unknown/decomposition products calculated based on the carbon balance was also lower than for the previous set of catalysts. Late (Zn) and post-transition metals (Pb, Sn) that are on the left side of the volcano plot ($\Delta G_H > 0$, see Figure 3) showed the highest ECH rates and among the highest selectivities to *t*3HDA. Notably, Pb hydrogenated *ct*MA to *t*3HDA with 90% selectivity at 70% conversion and 60% faradaic efficiency under these reaction conditions (Figure 5). The faradaic efficiency further increased to reach ∼100% when argon was bubbled to purge the reaction vessels and remove any dissolved oxygen that could react at the cathode (ORR). These results are consistent with previous reports on levulinic acid,[31] HMF,[27,30] and sorbitol hydrogenation,[28] which identified Pb as a promising electrocatalyst for biorenewable chemical conversion. In contrast, results obtained for Mo ($\Delta G_H < 0$) were markedly different and displayed trends similar to low

DOI: 10.1021/acssuschemeng.6b00679
ACS Sustainable Chem. Eng. 2016, 4, 3575−3585

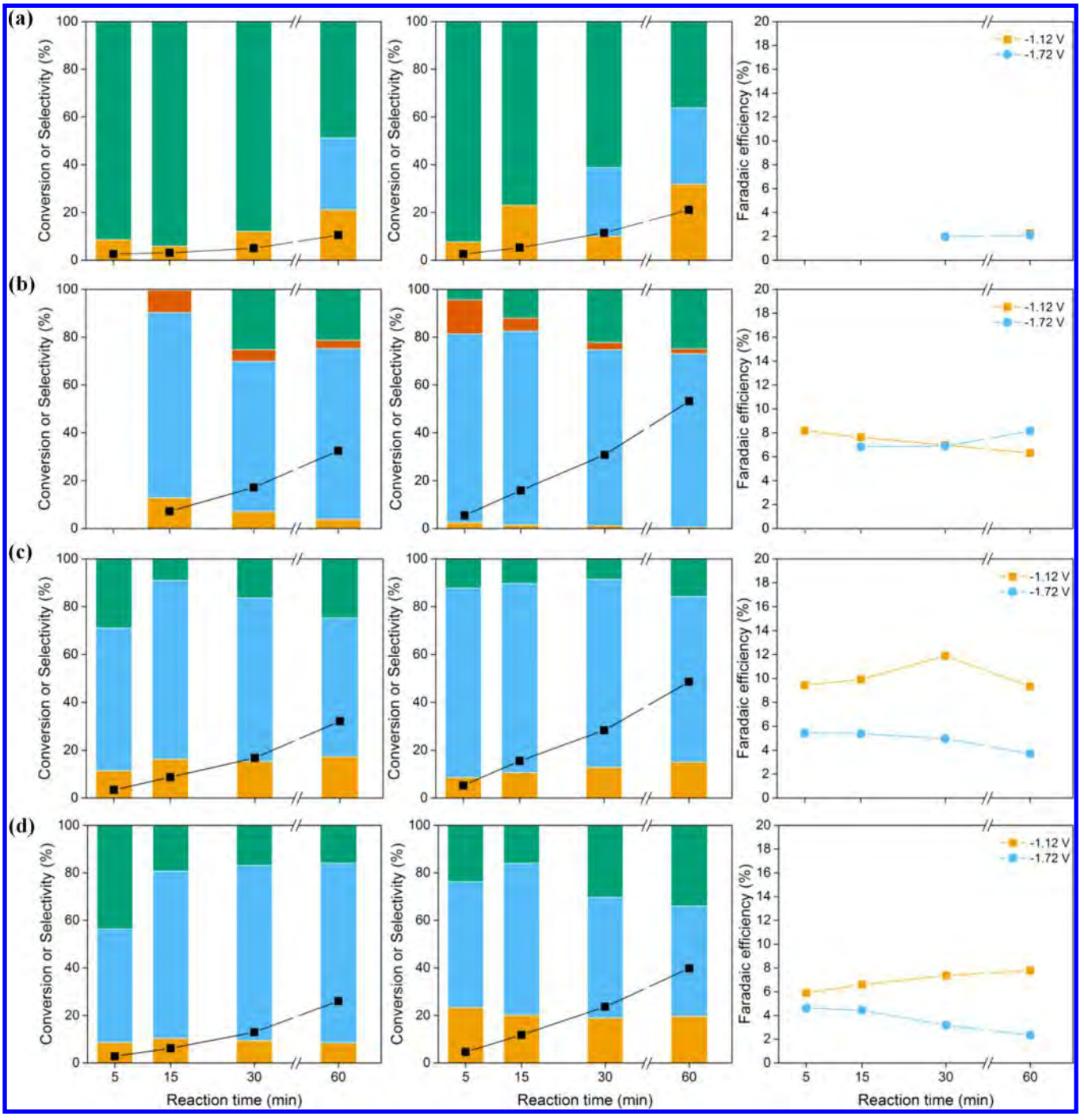

Figure 4. ECH of *ct*MA in 1% formic acid solution with low hydrogen overpotential metals at −1.12 V (left), −1.72 V (middle), and corresponding faradaic efficiencies (right). (a) Pd, (b) Ni, (c) Cu, (d) Fe. Legend: (black) *ct*MA conversion, (gold) *tt*MA selectivity, (blue) *t*3HDA selectivity, (red) AA selectivity, and (green) unknown/decomposition product selectivity.

hydrogen overpotential metals. It appears that strong hydrogen binding is detrimental to high ECH performance, probably due to competitive adsorption. This interpretation is supported by the trend observed for faradaic efficiency as a function of ΔG_H (Figure 3). However, the large binding strength of hydrogen to Mo appears to promote *tt*MA formation further suggesting electrochemical promotion of *ct*MA isomerization with electro-reduced protons on the surface of the electrode. It should be noted that clear trends between selectivity and hydrogen binding properties have not been identified in previous works. Often, the selectivity toward the desired product is only reported at low substrate conversion (<10%), which can be misleading as the selectivity can fluctuate significantly over the course of the reaction, even over short reaction times (Figure 5).

***ct*MA Electrocatalytic Hydrogenation Pathway.** Low and high hydrogen overpotential metals show significant differences in reaction rates, faradaic efficiency, and selectivity. The unknown compounds calculated based on the carbon balance could correspond either to additional hydrogenation products that could not be identified and quantified, or to decomposition products resulting from oxidation at the counter

DOI: 10.1021/acssuschemeng.6b00679
ACS Sustainable Chem. Eng. 2016, 4, 3575−3585

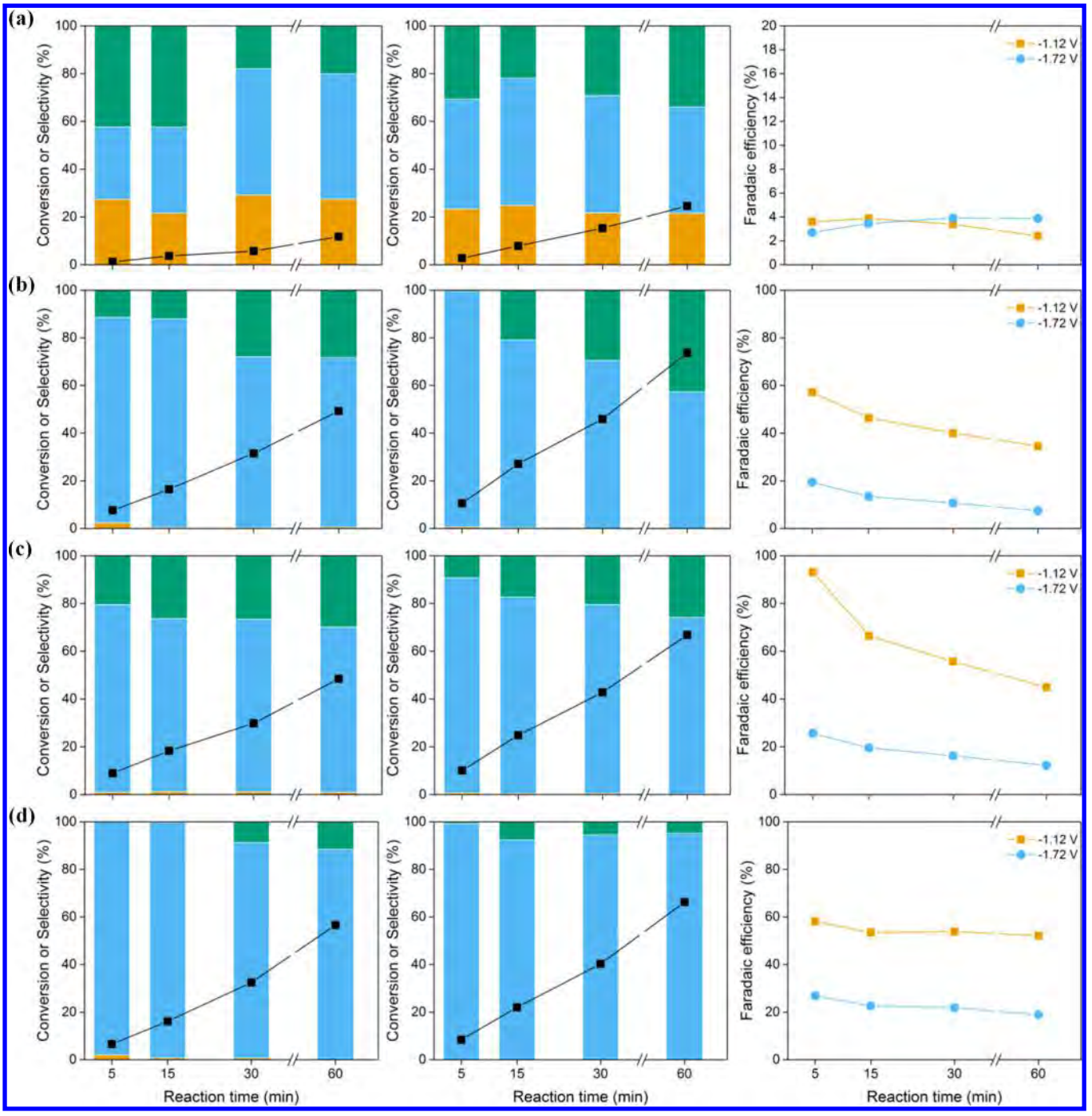

Figure 5. ECH of *ct*MA in 1% formic acid solution with high hydrogen overpotential metals at −1.12 V (left), −1.72 V (middle), and corresponding faradaic efficiencies (right). (a) Mo, (b) Sn, (c) Zn, and (d) Pb. Legend: (black) *ct*MA conversion, (gold) *tt*MA selectivity, (blue) *t*3HDA selectivity, (green) unknown/decomposition product selectivity.

electrode. To elucidate the reaction pathways in more detail for the reactions on Pb, we performed the same ECH at low cathodic potential (−0.57 V) to slow the kinetics and we monitored the reaction for 300 min (Figure 6a). Under these conditions, 57% selectivity toward *tt*MA was obtained after 60 min of reaction with the Pb electrode. Moreover, *tt*MA concentration decreased as *ct*MA conversion reached 80%, thus strongly supporting that *tt*MA is an intermediate in the hydrogenation of *ct*MA to *t*3HDA. This intermediate was not observed at higher potential (−1.12 and −1.72 V) likely due to faster kinetics or a shift in the rate-determining step (Figure 5).

The solution recovered after ECH of *ct*MA at −1.72 V was further analyzed by ^{1}H NMR. The spectrum displayed 96% yield to *t*3HDA instead of a racemic mixture of *cis* and *trans* isomers (Figure 6b). For catalysts that produce *t*3HDA, this indicates that *ct*MA is first electrochemically isomerized to *tt*MA followed by the ECH of *tt*MA to *t*3HDA (Figure 6c). It is interesting to note that the further hydrogenation of *t*3HDA to AA did not occur even with a 600 mV difference in cathodic potential. This could be due to the weaker binding of *t*3HDA with the metal electrode compared to *ct*MA and *tt*MA. Once *t*3HDA forms and desorbs no further hydrogenation occurs.

DOI: 10.1021/acssuschemeng.6b00679
ACS Sustainable Chem. Eng. 2016, 4, 3575−3585

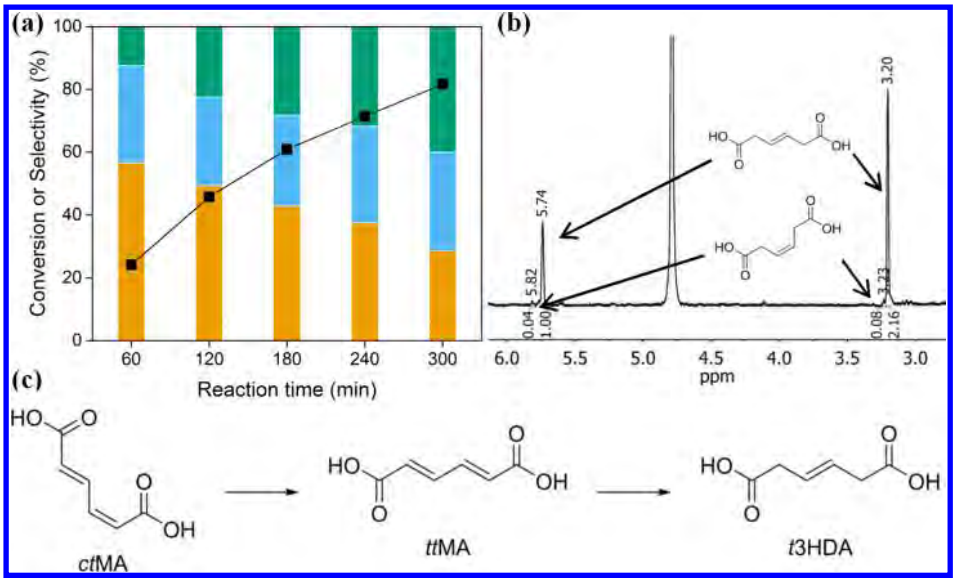

Figure 6. (a) ECH on Pb at −0.57 V of *ct*MA in a 0.01 M sulfuric acid solution. (black) *ct*MA conversion, (gold) *tt*MA selectivity, (blue) *t*3HDA selectivity, (green) unknown/decomposition product selectivity. (b) ^{1}H NMR spectrum of the reaction products obtained after ECH a −1.72 V; integrations of *c*3HDA and *t*3HDA correspond to 96% geometric isomer selectivity toward *t*3HDA. (c) Proposed reaction scheme for metals producing *t*3HDA.

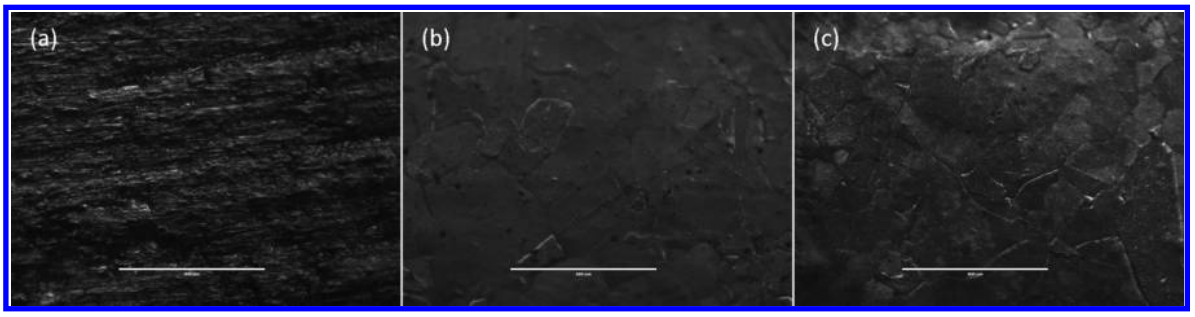

Figure 7. Light microscope images of the Pb electrode strip (a) after cleaning with a kimwipe, (b) after electropolishing, and (c) after ECH of *ct*MA. Scale bar: 400 μm.

The formation of intermediates in the production of AA on Ni are less clear. For high-pressure hydrogenation, it was determined that the hydrogenation of MA produced 2HDA followed by subsequent hydrogenation to AA.[12] This result suggests a mechanism involving a 1,2-addition followed by further hydrogenation to AA.[36] Surprisingly, 2HDA was never detected in our study. Instead, 60−80% of *t*3HDA, the product of the 1,4-addition, were found during the Ni-catalyzed ECH of *ct*MA. However, it should be noted that the carbon balance, shown as unknown/decomposition products in Figure 4, was relatively low for Ni. It is therefore possible that the reaction proceeds following two parallel pathways, leading to 2HDA by 1,2-addition and to 3HDA by 1,4-addition.

These two pathways are well-known in organic chemistry. For addition reactions on conjugated dienes, it has been established that the 1,2-adduct forms when the system is under kinetic control whereas the 1,4-adduct is obtained under thermodynamic control.[77] Therefore, this suggests that it could be possible to either enhance the formation of the kinetically- or thermodynamically favored hydrogenation product through variation of the applied potential and the choice in metal catalyst (e.g., selection by metal−hydrogen bond strength). Obviously, additional experiments are required to confirm this hypothesis, which is beyond the scope of the present work.

Electrochemically Active Surface Area and Turnover Frequency Calculations. Another important figure of merit for catalysts is the turnover frequency (TOF). Despite being a fair value to compare catalysts, TOFs are unusual in electrocatalysis because the electrochemically active surface area (ECSA) is difficult to determine in many cases. Nonetheless, we estimated the upper limit for the TOF with Pb catalyst, the most active and selective catalysts for the production of *t*3HDA.

Robust and accurate methods to determine the ECSA of Pb catalysts are not available yet. However, the electrode's geometric surface area can be used directly to estimate the catalyst's TOF if the surface is smooth. Optical microscopy images revealed microscopic features produced through wiping the soft metal with a Kimwipe (Figure 7a). Therefore, we electropolished the surface by immersing the Pb electrode into an acidic solution and applying a high potential. During this process, burs and sharp edges protruding from the electrode are dissolved into the electrolyte at a faster rate than the oblate material. After electropolishing, most of these features are leveled and the geometric area of the electrode strip was estimated to be the electrochemically active surface area (Figure 7b). The number of exposed metal atoms was then calculated using a reference value of 9.39×10^{14} atoms cm^{-2}.[78]

DOI: 10.1021/acssuschemeng.6b00679
ACS Sustainable Chem. Eng. 2016, 4, 3575−3585

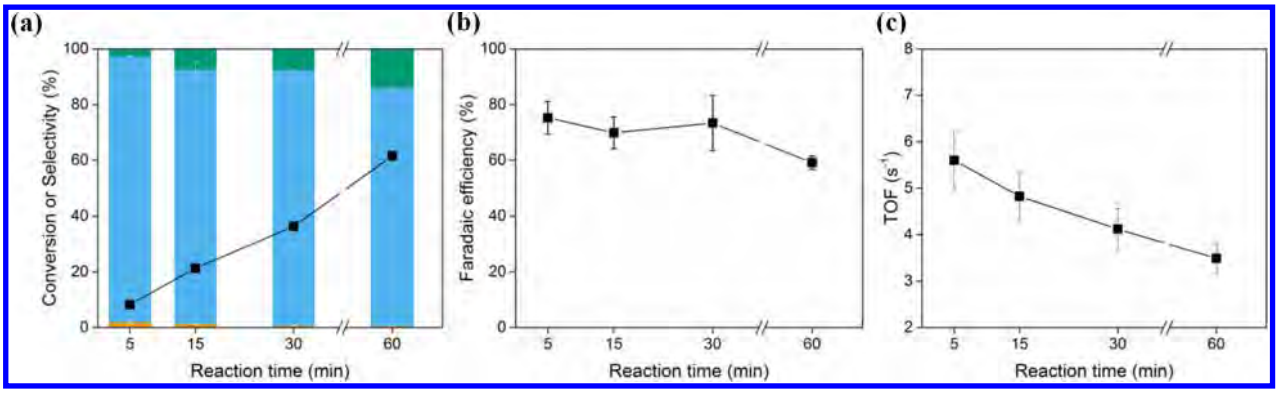

Figure 8. (a) ECH of *ct*MA with electropolished Pb at −1.17 V in a 1% formic acid solution (black) *ct*MA conversion, (gold) *tt*MA selectivity, (blue) *t*3HDA selectivity, (green) unknown/decomposition product selectivity, (b) faradaic efficiency, and (c) TOF of corresponding ECH.

After electropolishing, two consecutive ECHs of *ct*MA were carried out and the results were compared. Minor fluctuations in conversion, selectivity, faradaic efficiency, and TOF were calculated although the surface roughness increased (Figure 7c; error bars in Figure 8). The TOF was about 5.6 s^{-1} in the early stages of the catalytic tests (Figure 8c) in the absence of external mass transfer (Figure S3). This value seems reasonable considering that it is not based on the ECSA but on the geometric surface area of the electrode, and is therefore an upper limit estimate.

CONCLUSION

Biologically produced muconic acid emerges as a platform chemical for the synthesis of a wide range of biobased monomers. The production of adipic acid, a Nylon-6,6 precursor, through high pressure hydrogenation is already well established. Here, we explored the electrocatalytic hydrogenation of MA at room temperature and atmospheric pressure using hydrogen generated *in situ* from water. *ct*MA was converted to *tt*MA, AA, and *t*3HDA by applying a potential between −0.57 to −1.72 V on a transition metal catalyst. Conversion, selectivity, and faradaic efficiency were tuned largely by varying the experimental conditions, notably the nature of the metal and the applied potential. Metals that bind hydrogen weakly ($\Delta G_H > 0$), in particular Pb, were highly active and selective toward *t*3HDA, a promising monomer for bioadvantaged polyamides.[15] Conversely, catalysts that bind hydrogen more strongly were selective toward *tt*MA and displayed low faradaic efficiencies (Figure 3). The reaction appears to proceed through the intermediate *tt*MA, which itself is a precursor to biobased PET and can be obtained with a good selectivity by lowering the applied potential.

ASSOCIATED CONTENT

Supporting Information

The Supporting Information is available free of charge on the ACS Publications website at DOI: 10.1021/acssuschemeng.6b00679.

Calculation information, electrode surface areas, ^{1}H NMR spectrum of the target product, and reactant and product chromatograms (PDF).

AUTHOR INFORMATION

Corresponding Author

*J.-P. Tessonnier. E-mail: tesso@iastate.edu.

Notes

The authors declare no competing financial interest.

ACKNOWLEDGMENTS

This material is based upon work supported in part by the National Science Foundation Grant Numbers EEC-0813570, EPSC-1101284, and CBET-1512126. Research at the Ames Laboratory was supported by the U.S. Department of Energy-Laboratory Royalty Revenue through Contract No.DE-AC02-07CH11358. Work at The University of Alabama was supported by the Chemical Sciences, Geosciences and Biosciences Division, Office of Basic Energy Sciences, U.S. Department of Energy (catalysis center program). D.A.D. also thanks the Robert Ramsay Chair Fund and the STANCE project "Technology for a Sustainable Chemical Economy" (RG14648) of The University of Alabama for support. We would like to thank Dr. Sarah Cady (ISU Chemical Instrumentation Facility) for training and assistance pertaining to the AVIII-600 results included in this publication.

REFERENCES

(1) Choi, S.; Song, C. W.; Shin, J. H.; Lee, S. Y. Biorefineries for the production of top building block chemicals and their derivatives. *Metab. Eng.* **2015**, *28*, 223−239.

(2) Werpy, T.; Petersen, G. *Top Value Added Chemicals From Biomass. Volume I: Results of Screening for Potential Candidates from Sugars and Synthesis Gas*; DOE/GO-102004-1992; Department of Energy: Washington, DC, 2004.

(3) Bozell, J. J.; Petersen, G. R. Technology development for the production of biobased products from biorefinery carbohydrates-the US Department of Energy's "Top 10" revisited. *Green Chem.* **2010**, *12* (4), 539−554.

(4) Saha, B.; Abu-Omar, M. M. Advances in 5-hydroxymethylfurfural production from biomass in biphasic solvents. *Green Chem.* **2014**, *16* (1), 24−38.

(5) van Putten, R.-J.; van der Waal, J. C.; de Jong, E.; Rasrendra, C. B.; Heeres, H. J.; de Vries, J. G. Hydroxymethylfurfural, a versatile platform chemical made from renewable resources. *Chem. Rev.* **2013**, *113* (3), 1499−1597.

(6) Wang, T.; Nolte, M. W.; Shanks, B. H. Catalytic dehydration of C6 carbohydrates for the production of hydroxymethylfurfural (HMF) as a versatile platform chemical. *Green Chem.* **2014**, *16* (2), 548−572.

(7) Lane, J. *The DOE's 12 Top Biobased Molecules − What Became of Them?* http://www.biofuelsdigest.com/bdigest/2015/04/30/the-does-12-top-biobased-molecules-what-became-of-them/ (accessed August 6).

(8) Shanks, B. H. Unleashing biocatalysis/chemical catalysis synergies for efficient biomass conversion. *ACS Chem. Biol.* **2007**, *2* (8), 533−535.

DOI: 10.1021/acssuschemeng.6b00679
ACS Sustainable Chem. Eng. 2016, 4, 3575−3585

(9) Shanks, B. H. Conversion of biorenewable feedstocks: New challenges in heterogeneous catalysis. *Ind. Eng. Chem. Res.* **2010**, *49* (21), 10212−10217.
(10) Shanks, B. H. Across the board: Brent H. Shanks. *ChemSusChem* **2015**, *8* (6), 928−930.
(11) Schwartz, T. J.; O'Neill, B. J.; Shanks, B. H.; Dumesic, J. A. Bridging the chemical and biological catalysis gap: Challenges and outlooks for producing sustainable chemicals. *ACS Catal.* **2014**, *4* (6), 2060−2069.
(12) Vardon, D. R.; Franden, M. A.; Johnson, C. W.; Karp, E. M.; Guarnieri, M. T.; Linger, J. G.; Salm, M. J.; Strathmann, T. J.; Beckham, G. T. Adipic acid production From lignin. *Energy Environ. Sci.* **2015**, *8* (2), 617−628.
(13) Chia, M.; Schwartz, T. J.; Shanks, B. H.; Dumesic, J. A. Triacetic acid lactone as a potential biorenewable platform chemical. *Green Chem.* **2012**, *14* (7), 1850−1853.
(14) Niu, W.; Draths, K. M.; Frost, J. W. Benzene-Free synthesis of adipic acid. *Biotechnol. Prog.* **2002**, *18* (2), 201−211.
(15) Suastegui, M.; Matthiesen, J. E.; Carraher, J. M.; Hernandez, N.; Rodriguez Quiroz, N.; Okerlund, A.; Cochran, E. W.; Shao, Z.; Tessonnier, J. P. Combining metabolic engineering and electrocatalysis: Application to the production of polyamides from sugar. *Angew. Chem., Int. Ed.* **2016**, *55* (7), 2368−2373.
(16) Schwartz, T. J.; Shanks, B. H.; Dumesic, J. A. Coupling chemical and biological catalysis: a flexible paradigm for producing biobased chemicals. *Curr. Opin. Biotechnol.* **2016**, *38*, 54−62.
(17) Domaille, D. W.; Hafenstine, G. R.; Greer, M. A.; Goodwin, A. P.; Cha, J. N. Catalytic upgrading in bacteria-compatible conditions via a biocompatible aldol condensation. *ACS Sustainable Chem. Eng.* **2016**, *4* (3), 671−675.
(18) Beerthuis, R.; Rothenberg, G.; Shiju, N. R. Catalytic routes towards acrylic acid, adipic acid and caprolactam starting from biorenewables. *Green Chem.* **2015**, *17* (3), 1341−1361.
(19) Van de Vyver, S.; Roman-Leshkov, Y. Emerging catalytic processes for the production of adipic acid. *Catal. Sci. Technol.* **2013**, *3* (6), 1465−1479.
(20) Xie, N.-Z.; Liang, H.; Huang, R.-B.; Xu, P. Biotechnological production of muconic acid: current status and future prospects. *Biotechnol. Adv.* **2014**, *32* (3), 615−622.
(21) Vardon, D. R.; Rorrer, N. A.; Salvachua, D.; Settle, A. E.; Johnson, C. W.; Menart, M. J.; Cleveland, N. S.; Ciesielski, P. N.; Steirer, K. X.; Dorgan, J. R.; Beckham, G. T. cis,cis-Muconic acid: separation and catalysis to bio-adipic acid for nylon-6,6 polymerization. *Green Chem.* **2016**, DOI: 10.1039/C5GC02844B.
(22) Bui, V.; Lau, M. K.; Macrae, D. Methods for producing isomers of muconic acid and muconate salts. Patent WO2011085311 A1, July 14, 2011.
(23) Burk, M. J.; Osterhout, R. E.; Sun, J. Semi-synthetic terephthalic acid via microorganisms that produce muconic acid. Patent US20140302573 A1, October 9, 2014.
(24) Cavani, F.; Teles, J. H. Sustainability in catalytic oxidation: An alternative approach or a structural evolution? *ChemSusChem* **2009**, *2* (6), 508−534.
(25) Averesch, N. J. H.; Krömer, J. O. Tailoring strain construction strategies for muconic acid production in S. cerevisiae and E. coli. *Metab. Eng. Commun.* **2014**, *1* (0), 19−28.
(26) Frontana-Uribe, B. A.; Little, R. D.; Ibanez, J. G.; Palma, A.; Vasquez-Medrano, R. Organic electrosynthesis: a promising green methodology in organic chemistry. *Green Chem.* **2010**, *12* (12), 2099−2119.
(27) Kwon, Y.; de Jong, E.; Raoufmoghaddam, S.; Koper, M. T. M. Electrocatalytic hydrogenation of 5-Hydroxymethylfurfural in the absence and presence of glucose. *ChemSusChem* **2013**, *6* (9), 1659−1667.
(28) Kwon, Y.; Koper, M. T. M. Electrocatalytic hydrogenation and deoxygenation of glucose on solid metal electrodes. *ChemSusChem* **2013**, *6* (3), 455−462.
(29) Nilges, P.; Schroder, U. Electrochemistry for biofuel generation: production of furans by electrocatalytic hydrogenation of furfurals. *Energy Environ. Sci.* **2013**, *6* (10), 2925−2931.
(30) Kwon, Y.; Birdja, Y. Y.; Raoufmoghaddam, S.; Koper, M. T. M. Electrocatalytic hydrogenation of 5-Hydroxymethylfurfural in acidic solution. *ChemSusChem* **2015**, *8* (10), 1745−1751.
(31) Xin, L.; Zhang, Z.; Qi, J.; Chadderdon, D. J.; Qiu, Y.; Warsko, K. M.; Li, W. Electricity storage in biofuels: selective electrocatalytic reduction of levulinic acid to valeric acid or gamma-valerolactone. *ChemSusChem* **2013**, *6* (4), 674−686.
(32) Qiu, Y.; Xin, L.; Chadderdon, D. J.; Qi, J.; Liang, C.; Li, W. Integrated electrocatalytic processing of levulinic acid and formic acid to produce biofuel intermediate valeric acid. *Green Chem.* **2014**, *16* (3), 1305−1315.
(33) Green, S. K.; Lee, J.; Kim, H. J.; Tompsett, G. A.; Kim, W. B.; Huber, G. W. The electrocatalytic hydrogenation of furanic compounds in a continuous electrocatalytic membrane reactor. *Green Chem.* **2013**, *15* (7), 1869−1879.
(34) Li, Z. L.; Kelkar, S.; Lam, C. H.; Luczek, K.; Jackson, J. E.; Miller, D. J.; Saffron, C. M. Aqueous electrocatalytic hydrogenation of furfural using a sacrificial anode. *Electrochim. Acta* **2012**, *64* (0), 87−93.
(35) Chapuzet, J. M.; Lasia, A.; Lessard, J. Electrocatalytic hydrogenation of organic compounds. In *Electrocatalysis*; Lipkowski, J., Ross, P. N., Eds.; Wiley-VCH: New York, 1998.
(36) Elvidge, J. A.; Linstead, R. P.; Smith, J. F. Polyene acids. Part V. Catalytic semi-hydrogenation of the three isomeric muconic acids and comfirmation of their configurations. *J. Chem. Soc.* **1953**, *0*, 708−711.
(37) Bauccio, M. L. *ASM Metals Reference Book*, 3rd ed.; ASM International: Novelty, OH, 1993; pp 235−237.
(38) Paar, R. G.; Yang, W. *Density-Functional Theory of Atoms and Molecules*; Oxford University Press: New York, 1989.
(39) Becke, A. D. Density-functional thermochemistry. III. The role of exact exchange. *J. Chem. Phys.* **1993**, *98* (7), 5648−5652.
(40) Lee, C.; Yang, W.; Parr, R. G. Development of the colle-salvetti correlation-energy formula into a functional of the electron density. *Phys. Rev. B: Condens. Matter Mater. Phys.* **1988**, *37* (2), 785−789.
(41) Godbout, N.; Salahub, D. R.; Andzelm, J.; Wimmer, E. Optimization of gaussian-type basis sets for local spin density functional calculations. Part I. Boron through neon, optimization technique and validation. *Can. J. Chem.* **1992**, *70* (2), 560−571.
(42) Curtiss, L. A.; Redfern, P. C.; Raghavachari, K.; Rassolov, V.; Pople, J. A. Gaussian-3 theory using reduced Møller-Plesset order. *J. Chem. Phys.* **1999**, *110* (10), 4703−4709.
(43) Frisch, M. J.; Trucks, G. W.; Schlegel, H. B.; Scuseria, G. E.; Robb, M. A.; Cheeseman, J. R.; Scalmani, G.; Barone, V.; Mennucci, B.; Petersson, G. A.; Nakatsuji, H.; Caricato, M.; Li, X.; Hratchian, H. P.; Izmaylov, A. F.; Bloino, J.; Zheng, G.; Sonnenberg, J. L.; Hada, M.; Ehara, M.; Toyota, K.; Fukuda, R.; Hasegawa, J.; Ishida, M.; Nakajima, T.; Honda, Y.; Kitao, O.; Nakai, H.; Vreven, T.; Montgomery, J. A., Jr.; Peralta, J. E.; Ogliaro, F.; Bearpark, M. J.; Heyd, J.; Brothers, E. N.; Kudin, K. N.; Staroverov, V. N.; Kobayashi, R.; Normand, J.; Raghavachari, K.; Rendell, A. P.; Burant, J. C.; Iyengar, S. S.; Tomasi, J.; Cossi, M.; Rega, N.; Millam, N. J.; Klene, M.; Knox, J. E.; Cross, J. B.; Bakken, V.; Adamo, C.; Jaramillo, J.; Gomperts, R.; Stratmann, R. E.; Yazyev, O.; Austin, A. J.; Cammi, R.; Pomelli, C.; Ochterski, J. W.; Martin, R. L.; Morokuma, K.; Zakrzewski, V. G.; Voth, G. A.; Salvador, P.; Dannenberg, J. J.; Dapprich, S.; Daniels, A. D.; Farkas, Ö.; Foresman, J. B.; Ortiz, J. V.; Cioslowski, J.; Fox, D. J. *Gaussian 09*; Gaussian, Inc.: Wallingford, CT, 2009.
(44) Pictet, R. G. *Ann. Chem. Phys.* **1876**, *183*, 180−193.
(45) Trouton, F., IV On molecular latent heat. *Philos. Mag.* **1884**, *18* (110), 54−57.
(46) Hildebrand, J. H. The entropy of vaporization as a means of distinguishing normal liquids. *J. Am. Chem. Soc.* **1915**, *37* (5), 970−978.
(47) Lewis, G. N.; Randall, M. *Thermodynamics*; McGraw Hill: New York, 1961.

DOI: 10.1021/acssuschemeng.6b00679
ACS Sustainable Chem. Eng. 2016, 4, 3575−3585

(48) Waser, J. *Basic Chemical Thermodynamics*; W. A. Benjamin: New York, 1966.
(49) Vasiliu, M.; Guynn, K.; Dixon, D. A. Prediction of the thermodynamic properties of key products and intermediates from biomass. *J. Phys. Chem. C* **2011**, *115* (31), 15686−15702.
(50) Vasiliu, M.; Jones, A. J.; Guynn, K.; Dixon, D. A. Prediction of the thermodynamic properties of key products and intermediates from biomass. II. *J. Phys. Chem. C* **2012**, *116* (39), 20738−20754.
(51) Klamt, A. Conductor-like Screening model for real solvents: A new approach to the quantitative calculation of solvation phenomena. *J. Phys. Chem.* **1995**, *99* (7), 2224−2235.
(52) Klamt, A.; Jonas, V.; Bürger, T.; Lohrenz, J. C. W. Refinement and parametrization of COSMO-RS. *J. Phys. Chem. A* **1998**, *102* (26), 5074−5085.
(53) Klamt, A. *Quantum Chemistry to Fluid Phase Thermodynamics and Drug Design*; Elsevier: Amsterdam, 2005.
(54) Pye, C. C.; Ziegler, T.; van Lenthe, E.; Louwen, J. N. An implementation of the conductor-like screening model of solvation within the amsterdam density functional package — Part II. COSMO for real solvents. *Can. J. Chem.* **2009**, *87* (7), 790−797.
(55) te Velde, G.; Bickelhaupt, F. M.; Baerends, E. J.; Fonseca Guerra, C.; van Gisbergen, S. J. A.; Snijders, J. G.; Ziegler, T. Chemistry with ADF. *J. Comput. Chem.* **2001**, *22* (9), 931−967.
(56) SCM. *ADF2012, Theoretical Chemistry*; Vrije Universiteit: Amsterdam, The Netherlands, 2012.
(57) Becke, A. D. Density-functional exchange-energy approximation with correct asymptotic behavior. *Phys. Rev. A: At., Mol., Opt. Phys.* **1988**, *38* (6), 3098−3100.
(58) Perdew, J. P. Density-functional approximation for the correlation energy of the inhomogeneous electron gas. *Phys. Rev. B: Condens. Matter Mater. Phys.* **1986**, *33* (12), 8822−8824.
(59) Perdew, J. P. Density-functional approximation for the correlation energy of the inhomogeneous electron gas (Erratum). *Phys. Rev. B: Condens. Matter Mater. Phys.* **1986**, *34*, 7406−7406.
(60) Tomasi, J.; Mennucci, B.; Cammi, R. Quantum mechanical continuum solvation models. *Chem. Rev.* **2005**, *105* (8), 2999−3094.
(61) Klamt, A.; Schüürmann, G. COSMO: A new approach to dielectric screening in solvents with explicit expressions for the screening energy and its gradient. *J. Chem. Soc., Perkin Trans. 2* **1993**, No. 5, 799−805.
(62) Frisch, M. J.; Trucks, G. W.; Schlegel, H. B.; Scuseria, G. E.; Robb, M. A.; Cheeseman, J. R.; Montgomery, J. A., Jr.; Vreven, T.; Kudin, K. N.; Burant, J. C.; Millam, J. M.; Iyengar, S. S.; Tomasi, J.; Mennucci, B.; Cossi, M.; Scalmani, G.; Rega, N.; Petersson, G. A.; Nakatsuji, H.; Hada, M.; Ehara, M.; Toyota, K.; Fukuda, R.; Hasegawa, J.; Ishida, M.; Nakajima, T.; Honda, Y.; Kitao, O.; Nakai, H.; Klene, M.; Li, X.; Knox, J. E.; Hratchian, H. P.; Cross, J. B.; Bakken, V.; Adamo, C.; Jaramillo, J.; Gomperts, R.; Stratmann, M.; Yazyev, O.; Austin, A. J.; Cammi, R.; Pomelli, C.; Ochterski, J. W.; Ayala, P. Y.; Morokuma, K.; Voth, G. A.; Salvador, P.; Dannenberg, J. J.; Zakrzewski, V. G.; Dapprich, S.; Daniels, A. D.; Strain, M. C.; Farkas, Ö.; Malick, D. K.; Rabuck, A. D.; Raghavachari, K.; Foresman, J. B.; Ortiz, J. V.; Cui, Q.; Baboul, A. G.; Clifford, S.; Cioslowski, J.; Stefanov, B. B.; Liu, G.; Liashenko, A.; Piskorz, P.; Komaromi, R. L.; Martin, R. L.; Fox, D. J.; Keith, T.; Al-Laham, M. A.; Peng, C. Y.; Nanayakkara, A.; Challacombe, M.; Gill, P. M. W.; Johnson, B.; Chen, W.; Wong, M. W.; Gonzalez, C.; Pople, J. A. *Gaussian 03*, Revision E.01; Gaussian, Inc.: Wallingford, CT, 2004.
(63) Gutowski, K. E.; Dixon, D. A. Ab Initio prediction of the gas- and solution-phase acidities of strong Brønsted acids: The calculation of pKa values less than − 10. *J. Phys. Chem. A* **2006**, *110* (43), 12044−12054.
(64) Camaioni, D. M.; Schwerdtfeger, C. A. Comment on "accurate experimental values for the free energies of hydration of H+, OH-, and H3O+. *J. Phys. Chem. A* **2005**, *109* (47), 10795−10797.
(65) Zhan, C.-G.; Dixon, D. A. Absolute hydration free energy of the proton from first-principles electronic structure calculations. *J. Phys. Chem. A* **2001**, *105* (51), 11534−11540.
(66) Frost, J. W.; Miermont, A.; Schweitzer, D.; Bui, V. Preparation of trans,trans muconic acid and trans,trans muconates. Patent US8426639 B2, June 16, 2010.
(67) An, W. D.; Hong, J. K.; Pintauro, P. N.; Warner, K.; Neff, W. The electrochemical hydrogenation of edible oils in a solid polymer electrolyte reactor. I. Reactor design and operation. *J. Am. Oil Chem. Soc.* **1998**, *75* (8), 917−925.
(68) Greeley, J.; Jaramillo, T. F.; Bonde, J.; Chorkendorff, I.; Norskov, J. K. Computational high-throughput screening of electrocatalytic materials for hydrogen evolution. *Nat. Mater.* **2006**, *5* (11), 909−913.
(69) Sandström, A. G.; Almqvist, H.; Portugal-Nunes, D.; Neves, D.; Lidén, G.; Gorwa-Grauslund, M. F. *Saccharomyces cerevisiae*: a potential host for carboxylic acid production from lignocellulosic feedstock? *Appl. Microbiol. Biotechnol.* **2014**, *98* (17), 7299−7318.
(70) Mei, X.; Wolf, C. Neutral and ionic supramolecular structures of unsaturated dicarboxylic acids and acridine: Significance of molecular geometry and proton transfer. *Eur. J. Org. Chem.* **2004**, *2004* (21), 4340−4347.
(71) Trasatti, S. Work function, electronegativity, and electrochemical behaviour of metals. *J. Electroanal. Chem. Interfacial Electrochem.* **1972**, *39* (1), 163−184.
(72) Pourbaix, M. *Atlas of Electrochemical Equilibria in Aqueous Solutions*; Pergamon: Oxford, 1966.
(73) Beverskog, B.; Puigdomenech, I. Revised Pourbaix diagrams for copper at 25 to 300 degrees C. *J. Electrochem. Soc.* **1997**, *144* (10), 3476−3483.
(74) Beverskog, B.; Puigdomenech, I. Revised Pourbaix diagrams for zinc at 25−300 degrees C. *Corros. Sci.* **1997**, *39* (1), 107−114.
(75) Salazar, M.; Smotkin, E. S. Electrochemically promoted olefin isomerization reactions at polymer electrolyte fuel cell membrane electrode assemblies. *J. Appl. Electrochem.* **2006**, *36* (11), 1237−1240.
(76) Ploense, L.; Salazar, M.; Gurau, B.; Smotkin, E. S. Proton spillover promoted isomerization of n-Butylenes on Pd-black cathodes/Nafion 117. *J. Am. Chem. Soc.* **1997**, *119* (47), 11550−11551.
(77) Vollhardt, P.; Schore, N. Delocalized Pi Systems. In *Organic Chemistry Structure and Function*, 5th ed.; W.H. Freeman and Company: New York, 2007.
(78) Seo, M.; Kikuchi, N.; Fushimi, K.; Habazaki, H.; Narita, T.; Nakayama, T. Anodic behavior of nickel in acidic perchlorate solution containing Pb2+. *ECS Trans.* **2008**, *16* (52), 109−116.

DOI: 10.1021/acssuschemeng.6b00679
ACS Sustainable Chem. Eng. 2016, 4, 3575−3585

Supporting Information

Electrochemical Conversion of Muconic Acid to Biobased Diacids Monomers

John E. Matthiesen,[a,b,c] Jack M. Carraher,[a,b,c] Monica Vasiliu,[d] David A. Dixon,[d] and Jean-Philippe Tessonnier[a,b,c]*

[a] *Department of Chemical and Biological Engineering, Iowa State University, 618 Bissell Road, Ames, Iowa 50011, United States*

[b] *NSF Engineering Research Center for Biorenewable Chemicals (CBiRC), 617 Bissell Road, Ames, Iowa 50011, United States*

[c] *US Department of Energy Ames Laboratory, 2408 Pammel Drive, Ames, Iowa 50011, United States*

[d] *Department of Chemistry, The University of Alabama, Shelby Hall, Tuscaloosa, Alabama 35487, United States*

*E-mail: tesso@iastate.edu Phone +1 515-294-4595.

Total number of pages: 6
Total number of figures: 3
Total number of tables: 1

Calculations

Conversion, selectivity, faradaic efficiency, and turnover frequency are calculated as follows. n is the number of electrons transferred (2=HDA, 4=Adipic acid), I is the current transferred, t is the reaction time, V is the volume of the electrolyte, and F is Faraday's constant. *Cis,trans*-muconic acid (*ct*MA), *trans,trans*-muconic acid (*tt*MA), *trans*-3-hexenedioic acid (*t*3HDA), and adipic acid (AA). The initial *tt*MA concentration $[ttMA]_0$ was typically <7 μM.

$$ctMA\ \text{Conversion}\ (\%) = \left(1 - \frac{[ctMA]_t}{[ctMA]_0}\right) * 100 \quad (1)$$

$$t3HDA\ \text{Selectivity}\ (\%) = \frac{[t3HDA]_t}{[ctMA]_0 - [ctMA]_t} * 100 \quad (2)$$

$$AA\ \text{Selectivity}\ (\%) = \frac{[AA]_t}{[ctMA]_0 - [ctMA]_t} * 100 \quad (3)$$

$$ttMA\ \text{Selectivity}\ (\%) = \frac{[ttMA]_t - [ttMA]_0}{[ctMA]_0 - [ctMA]_t} * 100 \quad (4)$$

$$\text{Faradaic Efficiency}\ (\%) = \frac{([t3HDA]_t * 2 + [AA]_t * 4) * F * V}{I * t} * 100 \quad (5)$$

$$\text{TOF} = \frac{moles_{MAconverted}}{moles_{metal} * t} \quad (6)$$

Table S1. Geometric dimensions of the metal electrodes

Metal	Length (mm)	Width (mm)	Thickness (mm)	Area (cm^2)
Cu	22.0	12.7	0.3	5.7
Fe	22.6	13.0	0.6	6.2
Mo	15.5	13.2	0.1	4.1
Ni	20.8	12.7	0.9	5.8
Pd Foil	12	25	0.1	6.0
Pb	20.5	12.0	0.8	5.3
Pb (Electropolished)	20.5	11.5	0.7	5.1
Sn	22.0	13.4	0.7	6.3
Zn	20.8	11.6	0.3	5.0

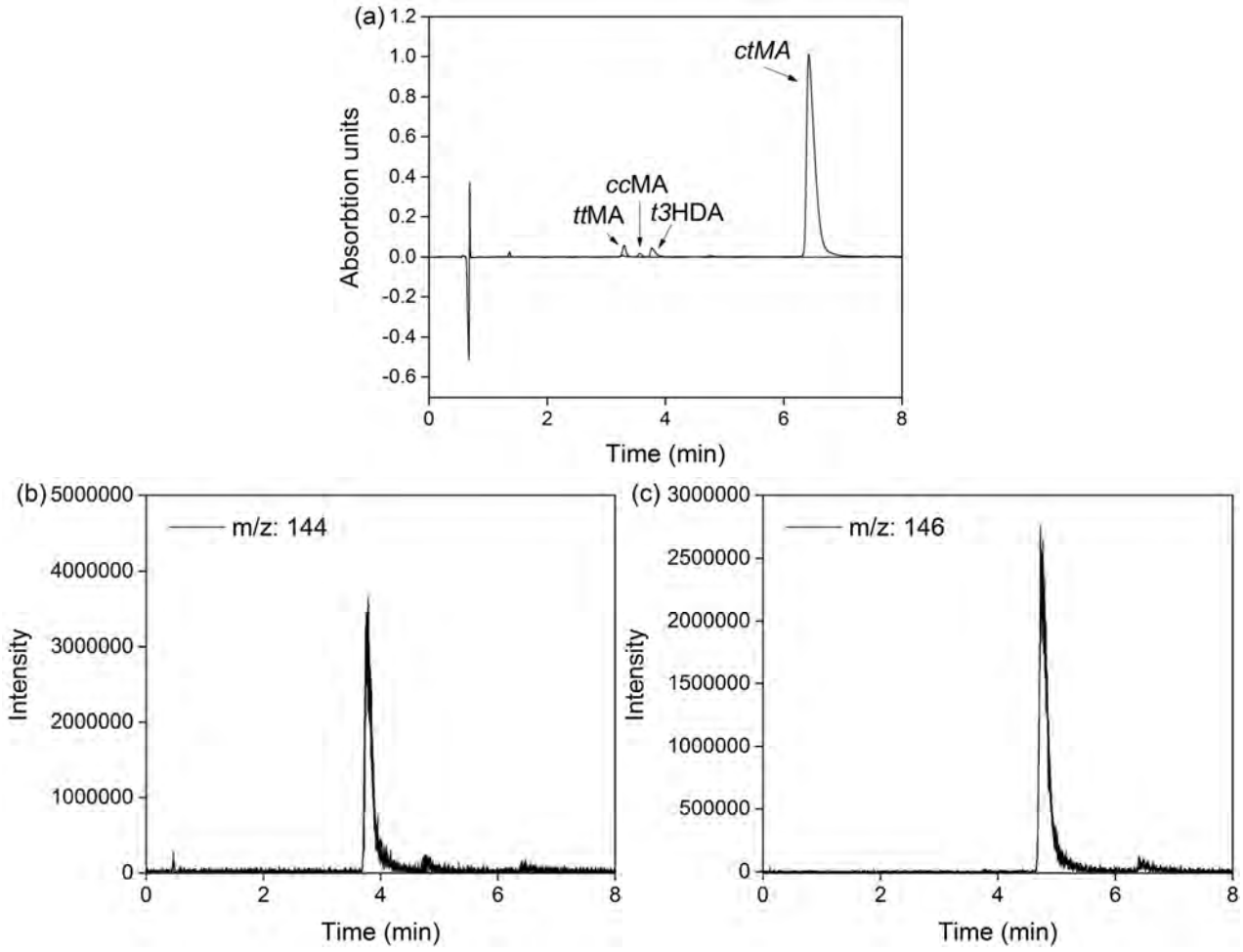

Figure S1. *ct*MA, *tt*MA, *t*3HDA, and AA UPLC elution times. Small quantities of *cc*MA (<1%) still remain in the reaction solution after thermal isomerization to *ct*MA. (a) 230 nm chromatograms of UPLC eluents. AA is a poor chromophore and does not appear in the chromatogram. (b) *m/z* =144 corresponding to *t*3HDA for QDa analysis and (c) *m/z* of 146 corresponding to AA for QDa analysis.

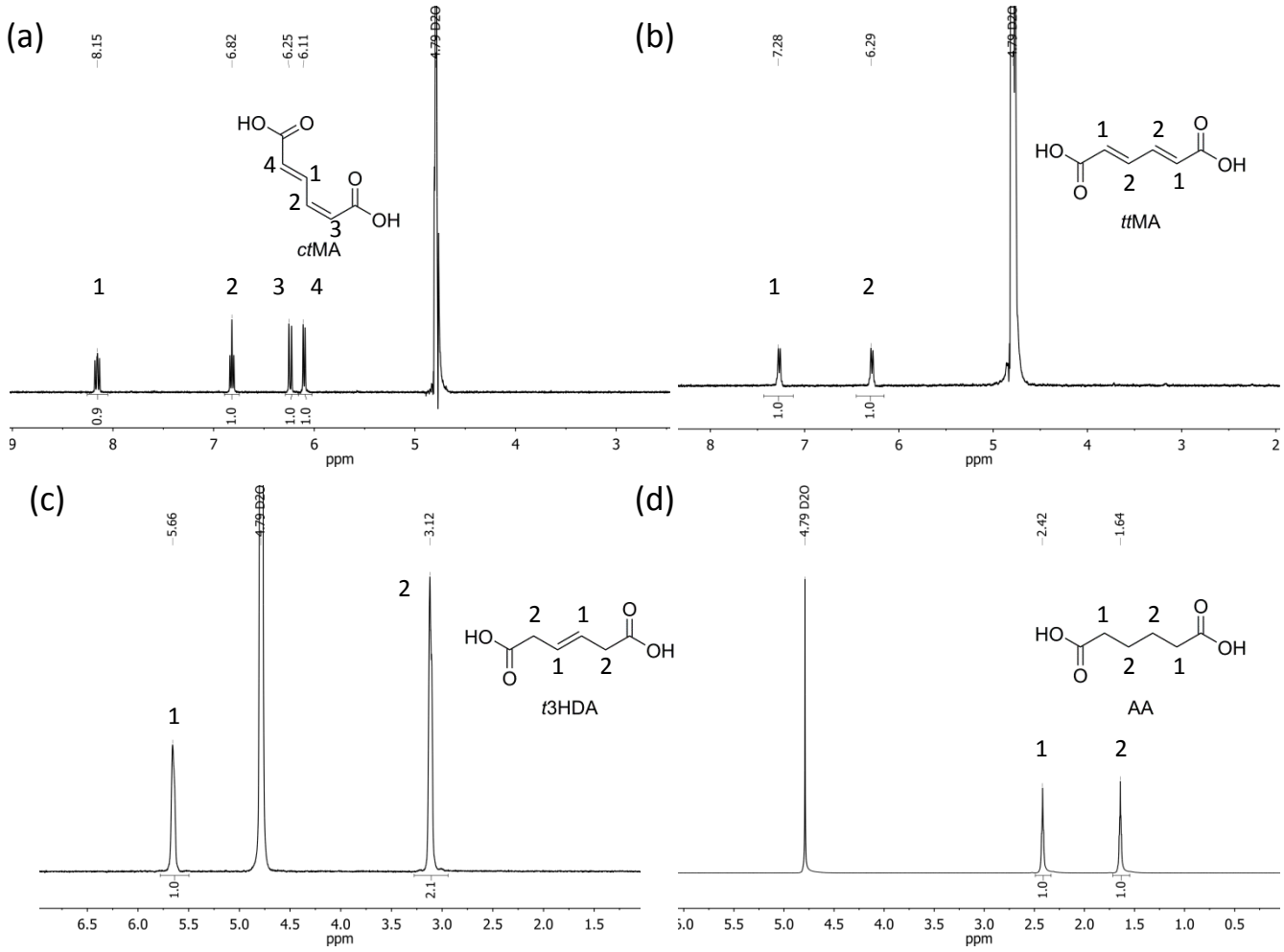

Figure S2. ^{1}H NMR spectra at 600 MHz in D_2O of genuine (a) *ct*MA, (b) *tt*MA, (c) *t*3HDA, and (d) AA

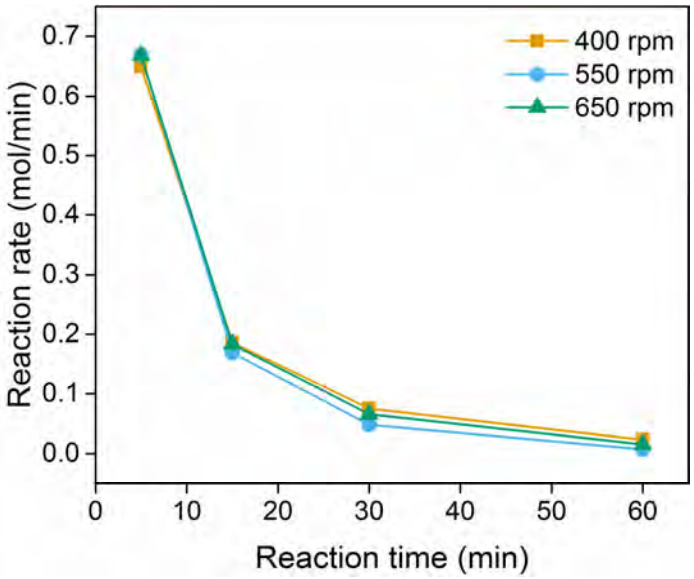

Figure S3. Effect of magnetic stirring of the solution on the reaction rate. The similarities between reactions rates obtained for different stirring rates suggest no influence of external mass transfer.